EFDA–JET–PR(14)35

R. Dejarnac, A. Podolnik, M. Komm, G. Arnoux, J.W. Coenen, S. Devaux,
L. Frassinetti, J.P. Gunn, G.F. Matthews, R.A. Pitts
and JET-EFDA Contributors

Numerical Evaluation of Heat Flux and Surface Temperature on a Misaligned JET Divertor W Lamella during ELMs

Numerical Evaluation of Heat Flux and Surface Temperature on a Misaligned JET Divertor W Lamella during ELMs

R. Dejarnac[1], A. Podolnik[1,2], M. Komm[1], G. Arnoux[3], J.W. Coenen[4], S. Devaux[5], L. Frassinetti[6], J.P. Gunn[7], G.F. Matthews[3], R.A. Pitts[8] and JET-EFDA Contributors*

JET-EFDA, Culham Science Centre, OX14 3DB, Abingdon, UK

[1]Institute of Plasma Physics, AS CR v.v.i., Prague, Czech Republic
[2]Department of Surface and Plasma Science, MFF Charles University, V Holešovičkách 2, 180 00 Prague, Czech Republic
[3]EURATOM/CCFE, Culham Science Center, Abingdon OX14 3DB, UK
[4]Institute of Energy and Climate Research–Plasma Physics, Forschungszentrum Juelich, Germany
[5]Max-Plank-Institute for Plasma Physics, Euratom Association, Garching, Germany
[6]Division of Fusion Plasma Physics, KTH, SE-10044 Stockholm, Sweden
[7]CEA, IRFM, F-13108 Saint-Paul-lez-Durance, France
[8]ITER Organization, Route de Vinon sur Verdon, 13115 St Paul-lez-Durance, France
** See annex of F. Romanelli et al, "Overview of JET Results", (24th IAEA Fusion Energy Conference, San Diego, USA (2012)).*

Preprint of Paper to be submitted for publication in
Nuclear Fusion

ABSTRACT

A series of experiments have been performed on JET to investigate the dynamics of transient melting due to Edge Localized Modes (ELMs). The experiment employs a deliberately misaligned lamella in one module of the JET bulk tungsten outer divertor, allowing the combination of stationary power flux and ELMs to transiently melt the misaligned edge. During the design of the experiment a number of calculations have been performed using 2D particle-in-cell (PIC) simulations and a heat transfer code to investigate the influence on the deposited power flux of finite Larmor radius effects associated with the energetic ELM ions. This has been done by parameter scans inside a range of pedestal temperatures and densities to scope different ELM energies corresponding to what was expected to be found in the experiment. On one hand, we observe optimistic results with the smoothing of the heat flux due to the Larmor gyration on the protruding side of the lamella that sees the direct parallel flux. Indeed, the deposited power tends to be lower than the nominal one on a distance smaller than 2 Larmor radii, which is always valid during ELMs for such a geometry. On the other hand, the fraction of the flux that does not reach the directly wetted side is transfered and spread to the top surface of the lamella. The hottest point of the lamella (corner side/top) does not always benefit from the gain from the larmor smoothing effect because of an enhanced power deposition from the second contribution.

1. MOTIVATIONS

Tungsten is the material that ITER will use for its divertor for the nuclear phase of operations. The energy stored in a typical ITER discharge achieving $Q_{DT} = 10$ in H-mode with 15MA of plasma current will be 350MJ [1]. Part of this energy will be periodically released in very short fractions of time during edge-localized modes (ELMs) as particle and heat fluxes. Power fluxes reaching the wall during ELMs or other transient events may exceed material limits if they cannot be mitigated and can lead to rapid damage like melting of metallic plasma facing components (PFCs). In order to assess the melting of metallic objects in tokamaks and its consequences, the fusion community has recently directed considerable effort into dedicated experiments and numerical modeling of melt dynamics and the effect of melting on tokamak operations. Tokamaks like AUG and JET changed all their PFCs from graphite/CFC to full W [2-5] and Tore Supra is now changing to a full metallic machine with the WEST project. Usually, PFCs which have the strongest interaction with the plasma have surfaces oriented with glancing angles to the magnetic field in order to spread the power over the widest possible area. However, in these high flux regions, the PFCs are generally castellated in order to withstand thermo-mechanical stress. The risk of melting comes mainly from edges due to mechanical misalignment between components. At these edges, the plasma impacts at near normal incidence on the material and deposited heat fluxes can increase by more than one order of magnitude. Using kinetic simulations, it has recently been shown, however, that in the case of high energy ions (such as those impacting on PFCs during ELM transients), the heat flux onto edges perpendicular to magnetic field lines can be reduced from the values expected geometrically

as a result of Larmor radius induced smoothing effects [6]. This reduction operates over a distance roughly equal to two Larmor radii. The question is then the following: which error do we make when we do not take into account the Larmor effect? To study the consequence of a possible melting, a dedicated melting experiment was performed on JET tokamak in summer 2013. A specially designed protruding tungsten lamella, with respect to its neighbors, was implemented in the JET divertor. The lamella was exposed to high power fluxes during a short time by moving the outer leg on the protruding edge for 1.5 s during high power JET pulses [7,8]. The melting occurred in 5 consecutive discharges. It was controlled by monitoring the surface temperature of the lamella by IR thermography to keep it below the melting point to avoid continuous melting and allow transient melting only during ELMs [9]. In this paper, we present a numerical study using the particle-in-cell (PIC) technique to estimate power deposition profiles on the side and top surfaces of the JET protruding lamella, combined to a simple 2D thermal model. The main aim being to understand heat fluxes expected on a protruding tile during large ELMs taking into account the Larmor gyration of the incoming ions and the consequent thermal response of the lamella. Indeed, the real heat flux is mainly coming from the side of the lamella and cannot be properly measured by the IR camera looking from above [9]. The different power flux scenarios in the simulations have been done by parameter scoping inside a range of experimental pedestal electron temperatures and densities to cover the ballpark of the expected ELM filament energy. The numerical model used for heat flux calculation as well as the geometry of the modeled misaligned lamella are presented in section 2 of this article. The results of the 2D power flux profiles on the protruding lamella surfaces are presented and discussed in section 3. The 2D thermal model, which was developed at the Institute of Plasma Physics (IPP) in Prague is detailed in section 4 of this article and results are presented. General conclusions are presented in section 5.

2. GEOMETRY AND NUMERICAL SET-UP

2.1. GEOMETRY

In the fist part of the study, we focus on the expected power deposition profiles on the side of the misaligned JET lamella. The geometry of the experiment is shown in Figure 1, illustrating how the misalignment gradually increases in the poloidal direction, presenting a progressively higher edge to the parallel heat flux, which impinges essentially perpendicularly on the protruding edge. This special lamella is installed in a single module of the JET bulk tungsten outer divertor, in a poloidal location (on “Stack A” of the module comprising 4 separate stacks of lamellae) which is not wetted by the outer strike point under normal operation [10]. The lamella is 62mm long in the poloidal direction and 5.9mm wide in the toroidal direction. The degree of protrusion varies linearly from 0.25mm to 2.5mm across the poloidal extent of the lamella. Several non-standard lamellae are also arranged in toroidally just before the special lamella to ensure that magnetic field lines are able to penetrate directly onto the misaligned edge (no self shadowing).

2.2. NUMERICAL SET-UP

Particle and power deposition profiles on perfectly aligned or misaligned monoblocks of castlellated PFCs can be simulated by means of PIC codes [6,11-13]. The electrostatic sheath and the magnetic pre-sheath, as well as the electric potential in the vicinity of the gaps between tiles play a major role in the plasma deposition in such geometry [14]. At this scale, the plasma is no longer quasi-neutral and the PIC technique can describe well the trajectories of charged particles in a self-consistent electric field. The code used here is a 2D-3V PIC code which was developed at IPP Prague in collaboration with CEA Cadarache. The electric field which accelerates the particles is derived from Poisson's equation at each time step. Ions are injected with an arbitrary velocity distribution function satisfying the Bohm criterion [15] and electrons are assumed to be Maxwellian. The case considered here is a fully ionized magnetized plasma with one species of singly charged ions (D^+) incident on a completely absorbing, conducting wall. The magnetic field is assumed constant, which is true to a high approximation on the very short distances (few mm) appropriate to this experiment and can have an arbitrary orientation. A magnetic sheath [16,17] can thus develop along the surface in the range of $4*r_L$, where r_L is the Larmor radius. This has been taken into consideration by ensuring a minimum distance of $10*r_L$ between the top of the tiles and the plasma-magnetic sheath boundary, thus avoiding any perturbation to the bulk plasma. The extent of the tile tops in the toroidal direction is also taken large enough to avoid perturbations generated by the gap itself due to the periodicity of the system. More details on the model can be found in [14].

The 2 dimensionality of the code forces that the modeled lamella must be semi-infinite in the poloidal direction with a constant protruding edge d with respect to the front lamella, as shown in Figure 2. In order to simulate the real lamella, we performed several simulations for different misalignments $d = 0.0, 0.5, 1.0, 1.5$ *and* $2.0mm$. PIC simulations are extremely time-consuming and have been performed on the super computer Helios in Rokkasho-Mura (Japan) on 16 processors. The length of one simulation varied in between 3 and 12 weeks according to the size of the simulation box and the plasma conditions. For the maximum protruding edge of $2.5mm$, the simulation box was too large to be modeled in any realistic amount of time. As it turned out, the real experiment did not push the strike point to the extreme location of highest misalignment and so such simulations are not necessary. To do so would have been challenging from an operational point of view at the high plasma currents which were eventually adopted for the experiment.

As it will be shown in section 3, it is in fact straightforward to extrapolate the modeling results to larger values of d without performing the full PIC simulation. The width of the gap between the lamella and its 2 neighbors is set to 1mm, the toroidal magnetic field is set to $B_t = 2.5T$ (its value at the radial position of stack A) and field lines impact the top surface with a shallow angle of $\alpha = 2.5^o$. Power deposition profiles are calculated on the side of the lamella (pink – Figure 2) and on the top surface (red – Figure 2). In the rest of the article we will refer to those 2 surfaces as the "side" and the "top" surfaces, respectively. These PIC simulations were conducted as part of the design of the JET lamella melting experiment and were thus performed before the actual experiment was

conducted. The model input parameters were specified on the basis of set-up plasmas executed before the misaligned lamella was installed in JET. The real plasma parameters used for the experiment (see Section 2.3) differed slightly from the set-up discharges, but were sufficiently close for the model input to be equally valid for the design phase and for interpretation of the experiments themselves.

2.3. ELM PLASMA PARAMETER SPECIFICATION

In the JET experiment, the actual melting was performed during a sequence of five 3MA pulses (JET Pulse Numbers 84778 to 84782) with a combined neutral beam plus ICRH heating power of 23MW. The resulting H-mode plasma had about 6MJ of total thermal energy and regular type I ELMs with energies around 0.3MJ. Within ~1s the base temperature of the lamella was raised to facilitate the melting by ELMs during the subsequent 0.5s. The special W lamella was monitored by local diagnostics including IR thermography systems. Plasma conditions are implemented in the code via electron density (n_e) and ion/electron temperatures (T_i/T_e) at the sheath entrance. Since it is difficult to estimate those quantities during type I ELMs (the ones which are most entitled to melt edges) we decided to study 3 different scenarios of ELM with different power in order to cover the whole ballpark of filament energies coming from the core plasma. Values of density and temperature were taken from the pedestal region in similar JET discharges as the ones expected for the melting experiment with type I ELMs.

We take 3 points in these profiles, at the top, middle and bottom of the pedestal, and we assume no parallel losses, so that those values are assumed to correspond to the ones at the sheath entrance of the lamella in the divertor at the strike-point location, and for the temperature we assume $T_e = T_i$. Under these conditions, the 3 simulated scenarios are summarized in Table 1 with the values of the resulting Larmor radius for D species and the nominal parallel flux $q_{//,0}$. Figure 3 shows the pedestal profiles of electron temperature (left) and density (right) given by High Resolution Thomson Scattering for one of the melting discharges, JET Pulse Number 84781, at 3 different times when the strike-point is moved to the special lamella. Values match the ones used to estimate the 3 different scenarios before the experiment (see Table 1). The assumptions used for calculating the scenarios are strong but we believe that for such fast, transient events they are realistic. Indeed, Figure 4 shows the temporal evolution of the spatial distribution of the parallel power density falling on the lamella during one ELM, measured by IR thermography of flat lamellae located just before the special lamella for JET Pulse Number 84779. Experimental fluxes range from 0.1 GW/m^2 to 3 GW/m^2, values which are covered by the 3 numerical scenarios.

3. POWER FLUX DEPOSITION PROFILES DURING ONE ELM

The PIC code calculations yield spatial profiles of the power flux deposition on (1) the protruding side of the lamella and (2) on the top surface. In the first part of this section, profiles related to point (1) are presented and discussed. Calculated power deposition profiles ($q_{//}^{PIC}$) as a function of protruding height and for the less severe scenario *S3* (see Table 1) are presented in Figure 5. Two

regions can be defined: negative x-axis values correspond to the protruding part of the special lamella, whilst positive x-values delimit the region inside the gap, thus below the level defined by the surface of the toroidally neighboring lamella which acts as the reference for the misalignment. For comparison, we have added on the graph the theoretical perpendicular flux that the top surface should see $q_{top\_surf} = q_{//,0} * sin(\alpha)$ and the almost parallel flux $q_{//} = q_{//,0} * cos(\alpha)$ (with $cos(\alpha) = 0.999$ for $\alpha = 2.5^{o}$) as it would be impacting the side of the lamella if we suppose no finite Larmor effect but a center-guide/ballistic approach and no electric field.

Inside the gap, the power deposition is rapidly damped with a fast exponential decay as already described in [18]. In the absence of finite Larmor radius effects, for a 1mm gap, the heat flux parallel to the field lines may only penetrate a distance of 0.044mm by geometric projection down below the surface of the neighboring flat lamella. The PIC simulations reveal that the deposited flux is lower than $q_{//}$ on the protruding side of the lamella. This optimistic result is the consequence of a smoothing effect due to the Larmor gyration of the incoming ions [6]. For a 2 mm misalignment, 95% of $q_{//}$ is reached, but only $0.5q_{//}$ for a protruding edge of 0.5mm. As shown in [6], a surface perpendicular to field lines must protrude by at least $2r_L$ if the full parallel heat flux is to be intercepted.

This is further illustrated by Figure 6, which is the analog of Figure 5 but for the ELM scenario *S1* in Table 1, with the highest ELM plasma temperature and hence the highest ion Larmor radius in the simulations. In this case, the smoothing effect increases, reducing the incident heat flux to 70% of $q_{//}$ at $d = 2mm$ and to only 35% at a misalignment of 0.5mm. By using the results of the full set of simulations (namely, the matrix of points obtained from the different values of d and ELM plasma temperature and density), a simple scaling law for the normalized heat flux deposited on the side of the lamella ($q_{//}^{PIC}/q_{//}$) as a function of the protruding part d normalized to the ion Larmor radius ($m = d/r_L$) can be derived. This scaling is shown in Figure 7 for the 3 ELM scenarios and is found to be linear ($q = a*m+b$), in the region of interest. These curves follow the same trend even for different Larmor radii. However, the contribution of the Larmor radius (and thus T_e) and n_e is also present in the coefficient a of the slope, which makes results difficult to extrapolate to other conditions and can explain the slight discrepancy observed between the curves. On the graph, the points corresponding to the maximum misalignment of the lamella ($d^{max} = 2.5\ mm$) are displayed. For scenarios *S1* & *S2*, at most ~ 80% of $q_{//}$ would be expected for the highest misalignment, whilst for the ELM parameters of scenario *S3* the parallel heat flux can actually be reached at full misalignment. It is important to note that simulations take no account of secondary electron emission (SEE). It was recently shown [19] that for surfaces almost perpendicular to the magnetic field, SEE can have strong consequences on the deposited power. The heat flux given here might thus be strongly underestimated. However, this will not change the ratio of deposited power to $q_{//}$ since SEE should affect the absolute values of all fluxes, including $q_{//}$.

The results for the calculated effective perpendicular power fluxes ($q_{\perp}^{PIC}$) falling on the top of the lamella for the ELM scenario *S3* are presented in Figure 8. The protruding lamella is located on the left of the gap for $y < 2.2mm$ (tile#2 on the schematic insert in Figure 8), with the reference lamella

corresponding to all $y > 3.2mm$ (tile#1) and the magnetic field lines are impacting from right to left. Due to the periodic boundary conditions used in the code, the left boundary being equal to the right one, the modeled geometry is equivalent to having a virtual, second protruding tile, or lamella, next to the reference tile, as it is illustrated in the second schematic insert in Figure 8. Care must be taken in choosing the size of the simulation box and a sufficient length of tile#1 so as to avoid artificial shadowing at the point of interest, i.e. the gap and the protruding lamella. Due to shallow angles, taking account for the entire box is not acceptable in terms of computation time, therefore the simulation box was optimized in order to have the artificial shadowing not farther than 2mm before the gap entrance. This is why the deposited power flux on tile#1 for $y > 5mm$ is lower than the nominal flux when the tiles are well aligned (here $q_{top\_surf} = 8MW/m^2$).

There is clearly an enhanced heat flux on the top surface of the misaligned lamella in comparison to the geometrically expected value. Moreover, the top surface heat flux profile peaks near the misaligned corner, with the degree of peaking increasing with increasing misalignment. The effect is due to the perturbation caused by the protruding edge, creating local electric fields which increase with increasing protrusion and attract ions (see Figure 9). The electric field is increased by a factor 2 from its value at zero misalignment (reference) to a misalignment of 2 mm, with a peaked value at the corner corresponding to 3 times the reference value. Although this effect can considerably enhance the top surface power flux density over that expected geometrically (by up to a factor 7.5 in Figure 8), it is still a small fraction of the parallel heat flux which is deposited on the lamella side, near the corner (Figure 5). A similar trend is found for ELM plasma cases *S1*, *S2* and a scaling can be defined for the top surface power deposition enhancement in a similar fashion to that performed for the side heat fluxes. Figure 10 shows the lamella top deposition power flux profiles normalized to q_{top_surf} as a function of the distance from the top surface normalized to the Larmor radius ($n = y/r_L$) for scenario *S2* and for the 4 simulated misalignments. The edge of the lamella corresponds to $n = 0$ and so that increasing n corresponds to increasing distance from the gap/edge.

The power deposition along the top surface clearly decreases with a double exponential decay. The first region corresponds to the peak value near the corner, in between points A and B on the graph. It has a short decay length, λ_{short}, over a short distance from the edge ($0.4*r_L$). The second region corresponds to more flattened profiles with a much larger decay length, λ_{long}, for the rest of the lamella top, between points B and C on the graph. The picture is similar for all the simulated scenarios, with $\lambda_{short} \sim 0.4r_L$. The power deposition profiles can thus more generally be characterized by the value of the peak at the corner, i.e. point A, and λ_{short}. The long decay length varies from 20 – 300 r_L and thus is essentially flat given the small extent of the lamella width (~6 r_L for ELM scenario *S3*).

Since the short decay length is constant for all the simulations ($\lambda_{short} = 0.55 \pm 0.02$) a scaling law is required only for the peaked top heat flux at the corner. The normalized power peak near the edge is plotted as a function of normalized misalignment for all ELM scenarios in Figure 11. The peaked value varies linearly with the misalignment and is similar for all ELM cases.

Having determined a scaled map for the deposited heat flux on the misaligned lamella contour, the temporal evolution of the surface temperature can be obtained by solving the heat equation. This is described in the following section.

4. TEMPORAL EVOLUTION OF SURFACE TEMPERATURE DURING ELMS

4.1. THE 2D THERMAL MODEL

The following 2D thermal model has been developed by the authors of this article and can be defined as a simple solver of the heat equation $\frac{dT}{dt} - \alpha \Delta T = q$, where T is the temperature function (in our case a two-dimensional matrix with time-dependent elements) and $\alpha = k/\rho c_p$ the thermal diffusivity (k = thermal conductivity, c_p = specific heat capacity, ρ = density). The variable q on the right hand side is the net external heat source, which is, in the case of the model here, the incoming plasma heat flux density onto the modeled surfaces. A discrete square grid and a finite difference numerical method are used, as well as an implicit scheme to solve the sparse matrix-defined system of linear equations. We assume that no other energy sources or radiation losses are present in the volume of the tile. This equation defines the declared sparse matrix when $T(t, x, y)$ is treated as a time-dependent vector with n_x x n_y elements.

At the boundaries, the temperature is kept constant. As the PIC outputs are in the form of surface heat flux, the flux q is related to the energy flux Q_s coming from the plasma through the surface of the grid element S, by the following equation: $q(x, y) = Q_s(x, y)*S/mc$ assuming that the flux does not change in time. The temperature in the empty space beneath the boundary of the tile material is taken constant in the direction of the flux intake, a conductive cooling of the lamella is thus simulated. The authors acknowledge that this model is not as efficient as commercial 3D codes but it has the advantage to run faster and to give trends, which have been well reproduced during transient events (ELMs) [20]. Moreover, uncertainties coming from incoming fluxes play a bigger role in the temperature output.

4.2. TEMPORAL EVOLUTION OF SURFACE TEMPERATURE PROFILES

The surface temperature of the lamella (T^{surf}) is calculated during ELMs using the PIC power flux profiles presented in section 3. The lamella is modeled by the following, constant material parameters corresponding to tungsten: $k = 173W/(m.K)$, $c_p = 130J/(kg.K)$, $\rho = 19250kg/m^3$ and the melting temperature is set at $T^{melt} = 3695K$. The temporal evolution of the ELMs is modeled by the function shown in Figure 13, which corresponds to the conditional averaged profile of the power flux measured by infra-red thermography in the ILW JET divertor. The starting temperature of the lamella (T^{base}) is a free parameter, set arbitrary to 2700K in the following simulations. During the melting experiment, the position of the strike point on the special lamella was at a poloidal location corresponding to a height of $d = 1.5mm$, therefore, corresponding power fluxes from the PIC simulations are used. Spatial profiles of T^{surf} on both surfaces of the lamella are presented in Figure 14 for the scenario *S2*. It has to be noted that for this specific case the Larmor smoothing,

i.e. the ratio $q^{PIC}/q_{//}$, is 60% on the side (see Figure 7 for $m = \sim 1$). In the present setup and for these conditions, the melting point was reached 1 ms after the start of the ELM.

The side of the lamella is mainly heated on its entire protruding edge (Figure 14 - left) with an increasing temperature towards the corner ($\Delta T^{side} \sim 400K$ over 1.5mm), whilst the top has a rather constant temperature on the whole surface, except at the corner B where there is a rapid increase of the order of $\Delta T^{top,corner} \sim 450K$ within 0.5mm (Figure 14 - right). The latter effect is due to the corner being also heated from the side by the incident flux in the parallel direction, which is much higher in absolute value than the flux falling on the top. The influence of the peaked flux as seen in Figure 8 also contributes to this sharp increase but marginally (it accounts only for 100K on the 1ms curves).

As a comparison, Figure 15 shows the same plots as in Figure 14 but for the center-guide/ballistic case when the Larmor smoothing effect is not taken into account using the nominal parallel flux $q_{//,0}*cos(\alpha)$ and $q_{//,0}*sin(\alpha)$ on the side and top surfaces, respectively.

Profiles are flat along the whole lamella on the side and on the top (both surfaces see a spatially constant flux) except at the top-corner where a strong peaking is observed. The increase at the corner of the top side is $\Delta T^{top,corner} \sim 950K$ over 0.5mm, so a rise of ~ 2 times the PIC case. There is also a negligible increase of the temperature at the side-corner of about 100K, which is due to the additional contribution from the perpendicular flux from the top always present at this transitional location. The main difference between those 2 profiles lies on T^{surf} absolute values. The side temperature in the center-guide/ballistic case is ~600K higher that the spatial averaged side temperature of the PIC case for a maximal ΔT of 1000K from the base temperature. This difference in spatial deposition profiles is the clear signature of the Larmor smoothing effect. The corner temperature appears to follow this trend too. The temporal evolution of the temperature of the lamella's hottest point during the ELM is plotted for both PIC and center-guide/ballistic cases for the same scenario *S2* and $d = 1.5mm$ in Figure 16.

1ms after the start of the ELM, the difference between the PIC and the center-guide/ballistic temperatures is ~ 400K for a maximum ΔT of 1000K in the case of center-guide/ballistic simulation, i.e. for the PIC case the corner temperature represents ~ 60% of the maximum increase in T^{surf}, value which is similar to the Larmor smoothing for these conditions (60%). Generally for all the scenarios, this trend is observed, even in the case of *S3* where the melting temperature is not reached after 1 ELM, the difference in the corner temperatures follows the power flux Larmor smoothing. The main difference concerns the spatial distribution of T^{surf} along the side, as shown in Figures 14 & 15, but for melting concerns, the important point to monitor is the corner where a sharp rise of T^{surf} is observed. At this particular point, the total flux is a combination of the 2 components of the flux, parallel and perpendicular, which corresponds to the maximum flux falling on the object independently of the heat flux spatial distribution farther from this point. In the PIC case, the perpendicular flux is furthermore enhanced with respect to the theoretical perpendicular flux. The absolute value depends on a particular geometry (protruding edge) and the plasma scenario (Larmor

radius), therefore this effect has to be assessed more generally for all cases including contributions from both side and top. A scaling of the total heat flux falling on the corner can be derived as a function of the misalignment normalized by r_L. The total incoming flux in both PIC and center-guide/ballistic cases using Figures 5 & 8 at the corner satisfies the following equation:

$$q_{//,0}*cos(\alpha) + q_{//,0}*sin(\alpha)\ (= q_{//} + q_{top\_surf}) \approx q_{//}^{PIC} + q_{\perp}^{PIC},$$

with $q_{//}^{PIC}$ and $q_{\perp}^{PIC}$ being the power fluxes given by the PIC calculations falling on the side and top, respectively.

Using scaling formulas shown in Figures 7& 11 for the side and top profiles, the flux falling on the corner normalized by $q_{//}$ can be described as follows:

$$\boldsymbol{q^{corner}/q_{//}} = (q_{//}^{PIC}+q_{\perp}^{PIC})/q_{//} = q_{//}^{PIC}/q_{//}+q_{\perp}^{PIC}/q_{//} = q_{//}^{PIC}/q_{//}+q_{\perp}^{PIC}/(q_{top\_surf}/sin(\alpha)) = \boldsymbol{q_{//}^{PIC}/q_{//}+(q_{\perp}^{PIC}/q_{top\_surf})}*sin(\alpha)$$

This scaling is presented in Figure 17 for the 3 ELM scenarios. The curves have a linear dependence until they reach the limit value of $q_{//}$, which is the maximum energy available in the system. Therefore, values greater than one (grey area) are non-physical and the power flux falling at the corner is thus $q_{//}$. The flux at the corner is at best $\sim q_{//}*40\%$ for the minimal misalignment of the experimental lamella ($d^{min} = 0.25mm \rightarrow m \sim 0$) for all scenarios. For scenarios *S1* & *S2*, curves reach the nominal parallel flux for a misalignment $d > 2mm$ but for the experimental misalignment of $d = 1.5mm$ (squares in Figure 17), points lie in the region where the Larmor smoothing is effective (~ 80%). For scenario *S3*, even for the experimental misalignment, the corner sees the full parallel flux and does not benefit of any smoothing effect for a misalignment greater than 1.3mm ($m = 1.6$), however, ELM filaments with such a low energy are unlikely to melt the W lamella.

PIC calculations define 2 regions where the effective Larmor smoothing effect is fully efficient or not with respect to the finite misalignment of the lamella. However, this corresponds to an ideal case where the corner is sharp and with no change in its geometry in time. In reality, because of high fluxes and a sharp edge, the corner's shape will be modulated by plasma surface interactions after few ELMs and hence, will not have its face strictly perpendicular to magnetic field lines. This make us conclude that values presented in Figure 17 are upper values and we believe that the smoothing effect should be more slightly more efficient for beveled edges.

5. CONCLUSIONS

The JET melting experiment (M13-01/02) was the main motivation of this study to investigate the power deposition profiles on a special misaligned lamella by means of particle-in-cell simulations during ELMy conditions. The goal was to predict and understand which physical processes are involved in the power deposition profiles on a perpendicular surface in the order of the ion Larmor radius during energetic ELMs. Simulations show that the power deposition profiles on the protruding

side of the lamella are lower than the expected nominal parallel flux thanks to the Larmor smoothing effect which is effective when the edge is protruding by a distance smaller than $2r_L$. The power deposition profiles on the top of the lamella are on the contrary higher than the classical, spread heat flux due to grazing angles on the flat top surface. As expected, the corner of the lamella, which represents the transitional point between the 2 surfaces, is a candidate for melting. Indeed, the part of the power which is not deposited on the side of the lamella is deposited on the top because of strong electric fields along the protruding surface. Scaling laws have been derived to describe the power deposition profiles for both surfaces, and therefore at the corner, as a function of the protruding distance normalized to the Larmor radius. Profiles are linear and thus seem to be independent of the ELM conditions. The power falling on the corner can be of 2 categories: one where the corner benefits form the Larmor smoothing effect (for large ELMs and small edges) and one where the corner does not benefit from this effect and sees the full parallel flux (for small ELMs and larger edges). A 2D in-house thermal code solving the heat equation was used to calculate the temporal evolution of the surface temperature spatial profiles. The lamella is mainly heated on its side and the corner between the side and the top corresponds to the hottest point, as it was expected. Despite the enhanced peaked flux coming from the top, the corner temperature seems to be not much affected (less than 10%). The surface temperature seems to follow the Larmor smoothing effect derived for the power flux on the side of the lamella. However, it has to be noted that the thermal model used in this study is basic and deeper investigation will be done using a more elaborated 3D thermal code [20]. However, from the experimental point of view, t he best diagnostic to compare our simulations with is the surface temperature given by IR measurements rather than the power flux of the filaments which are difficult to measure with good precision. This shows the difficulties to interpret experimental results. Nevertheless, this study mainly focuses on the physics of the distribution of power around a protruding edge in a castellated PFC rather than giving calibrated predictions. The main result of this numerical study shows a competition between large ELMs with a large smoothing effect versus small ELMs and no smoothing. This result might support the decision to protect the edges in the ITER divertor, even though larger ELMs, which tend to be responsible for the melting, should be the ones that are the most affected by the Larmor smoothing effect. Finally, results shown here are for a perfectly perpendicular corner but it is expected that after several ELMs the lamella edge will be beveled. This will change the power deposition at the corner itself in a more optimistic way. We therefore believe that numbers presented here are upper values but more 2D (or better 3D) additional PIC simulations with chamfered corners would be needed to assess this from a quantitative point of view.

ACKNOWLEDGMENTS

The authors would like to acknowledge Dr. Ph. Mertens for detailed description of the special misaligned lamella geometry, as well as the whole diagnosed stack A in JET and Dr. Y. Corre & Dr. B. Bazilev for fruitful discussions about surface temperature data interpretation from both experimental and numerical simulations point of view.

REFERENCES

[1]. Pitts R. A. et al., Journal of Nuclear Materials 415 (2011) pp. S957-S964

[2]. Neu R et al., Plasma Physics and Controlled Fusion 53, no. 12 (2011) 124040

[3]. Neu R, IEEE Transactions on Plasma Science, vol. 38, no. 3, March 2010, pp. 453–460

[4]. Thomser C et al., Fusion Science and Technology 62, no. 1 (2012) pp. 1-8

[5]. Matthews G F et al., Journal of Nuclear Materials 438 (2013) pp. S2-S10

[6]. Dejarnac R et al., Journal of Nuclear Materials 415 (2011) pp. S977-S980

[7]. Coenen J W et al., 'ELM induced W melting and its impact on tokamak operation', invited paper at the 21st International Conference on Plasma Surface Interactions, May 2014

[8]. Matthews G F et al., ''Melting of Tungsten by ELM Heat Loads in the JET Divertor, paper submitted to the 25th IAEA Fusion Energy Conference, October 2014.

[9]. Arnoux G et al., 'Thermal response up to melting of the exposed edge of a W lamella in the JET divertor', to be presented at the 21st International Conference on Plasma Surface Interactions, May 2014

[10]. Mertens P et al., Journal of Nuclear Materials 415 (2011) pp. S943-S947

[11]. Dejarnac R et al., IEEE Transactions on Plasma Science, vol. 38, no. 4, April 2010, pp. 1042–1046

[12]. Komm M et al., Plasma Physics and Controlled Fusion 53 (2011) 115004

[13]. Komm M et al.,Plasma Physics and Controlled Fusion 55 (2013) 025006

[14]. Dejarnac R et al., Journal of Nuclear Materials 363–365 (2007) pp. 560-564

[15]. J P Gunn, Journal of Nuclear Materials 337–339 (2005) p. 310

[16]. R Chodura, Physics of Fluids 25 (1982) p. 1628

[17]. J P Gunn, Physics of Plasmas 4 (1997) p. 4435

[18]. Dejarnac R et al., Journal of Nuclear Materials 390-391 (2009) pp. 818–821

[19]. Gunn J. P., Plasma Physics and Controlled Fusion 54 (2012) 085007

[20]. Bazylev B, Private communication

	$n_e\,[m^{-3}]$	$T_e = T_i\,[eV]$	$r_L\,[mm]$	$q_{//,0}\,[GW/m^2]$
Scenario 1 *(S1)*	7.10^{19}	500	1.8	7.10
Scenario 2 *(S2)*	4.10^{19}	300	1.4	1.90
Scenario 3 *(S3)*	2.10^{19}	100	0.8	0.18

Table 1: Summary of the three different ELM scenarios simulated with given input density and temperatures and resulting Larmor radius (r_L) and nominal parallel flux ($q_{//,0}$)

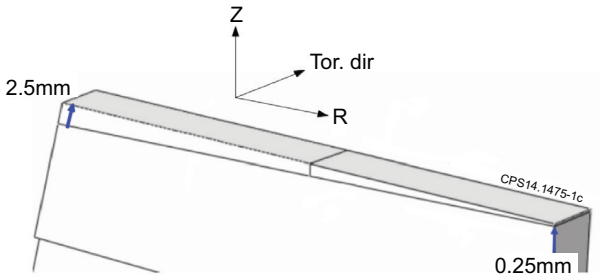

Figure 1: Schematic of the special protruding lamella in the JET divertor [10]

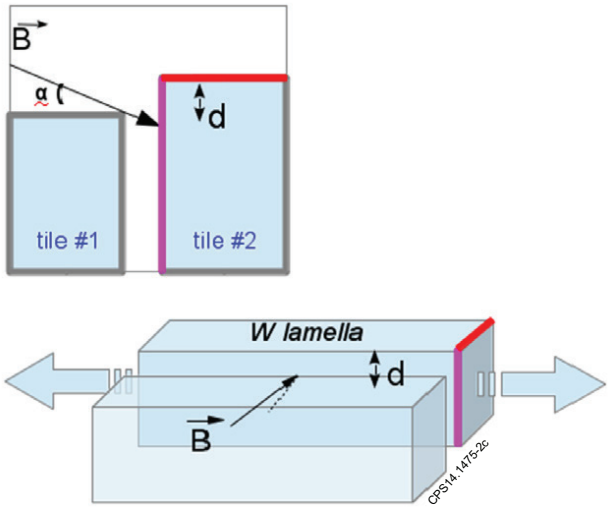

Figure 2: Schematic of the (semi-infinite) lamella as modeled in the 2D PIC simulations

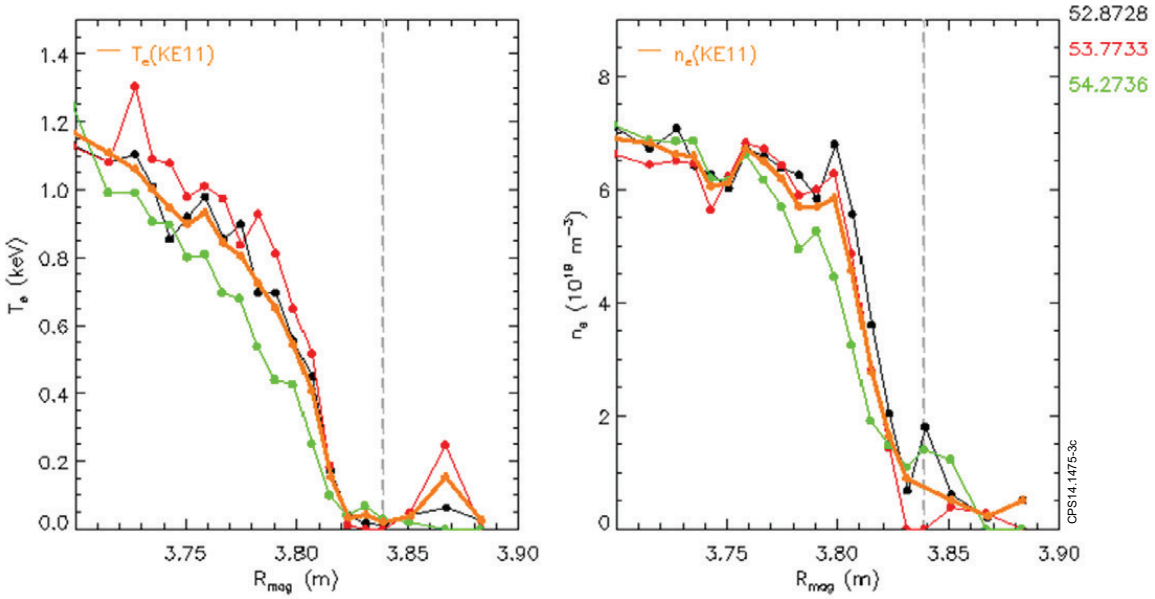

Figure 3: Pedestal profiles of electron temperature (left) and density (right) given by Thomson scattering for 1 of the 5 melting discharges (JET Pulse Number 84781) at 3 different times corresponding to the lamella exposure to high heat loads

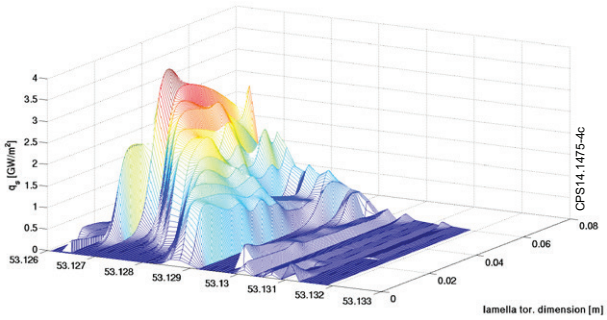

Figure 4: Temporal evolution of the spatial distribution of the power density falling on the lamella during one ELM, measured by IR thermography for 1 of the 5 melting discharges (JET Pulse Number 84779)

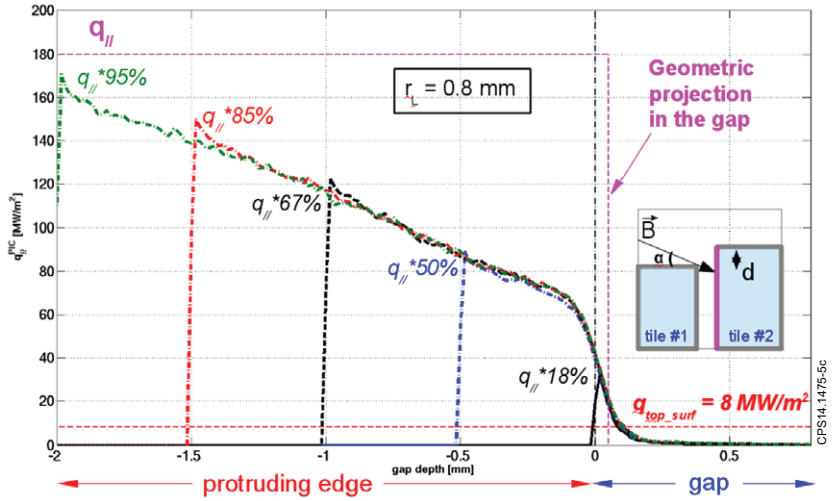

Figure 5: Power deposition profiles along the misaligned lamella side (including down below the surface defined by the neighboring lamella) for scenario S3 and 4 simulated misalignments. The theoretically expected power fluxes on the top surface and the parallel heat flux in the absence of any finite Larmor radius effects are marked for comparison

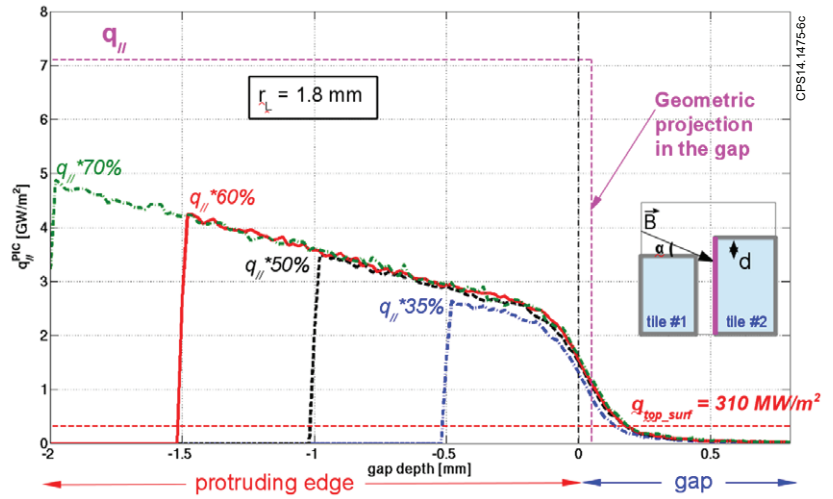

Figure 6: Power deposition profiles along the misaligned lamella side (including down below the surface defined by the neighboring lamella) for scenario S1 and 4 simulated misalignments. The theoretically expected power fluxes on the top surface and the parallel heat flux in the absence of any finite Larmor radius effects are marked for comparison

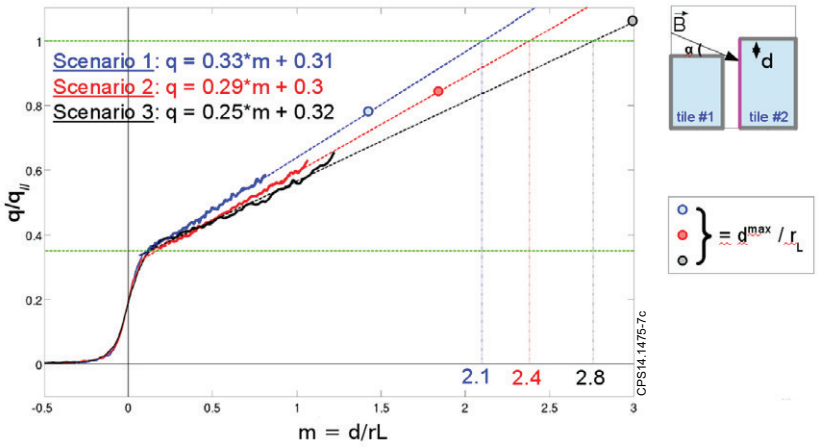

Figure 7: Scaling of the power deposition profiles on the lamella side (normalized to $q_{//}$) as a function of the misalignment normalized to r_L

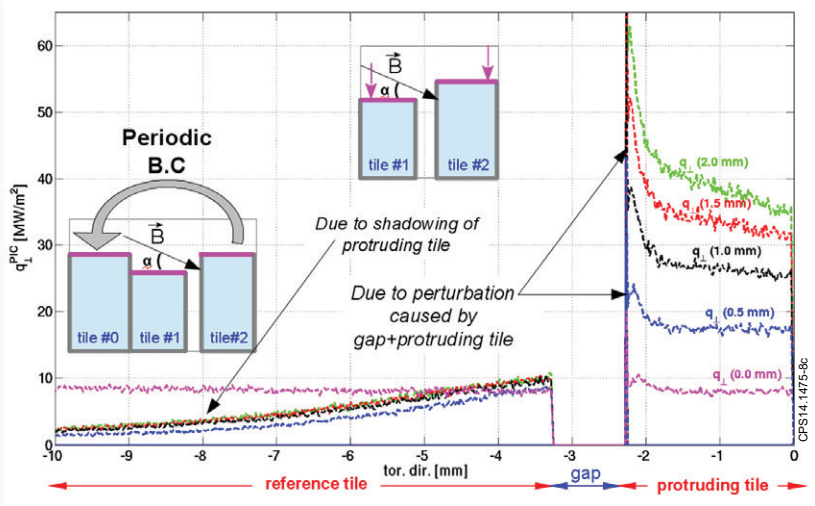

Figure 8: Power deposition profiles on the top surface of the lamella for scenario S3 and the 4 simulated misalignments

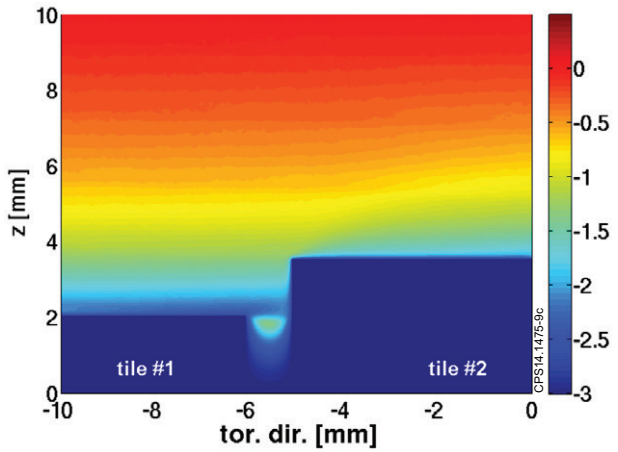

Figure 9: Electric field at the side of the lamella from the bottom of the gap to the top corner for 2mm protruding distance computed by 2D PIC calculations

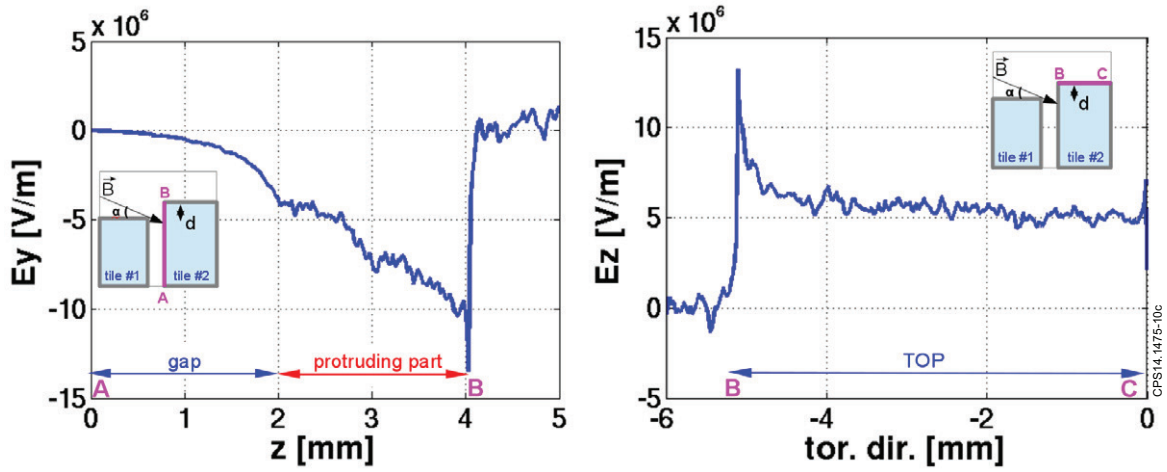

Figure 10: Spatial profiles of the power flux deposition normalized to q_{top_surf} as function of the distance normalized to r_L on the top surface of the lamella for ELM scenario S2 and for the 4 simulated misalignments

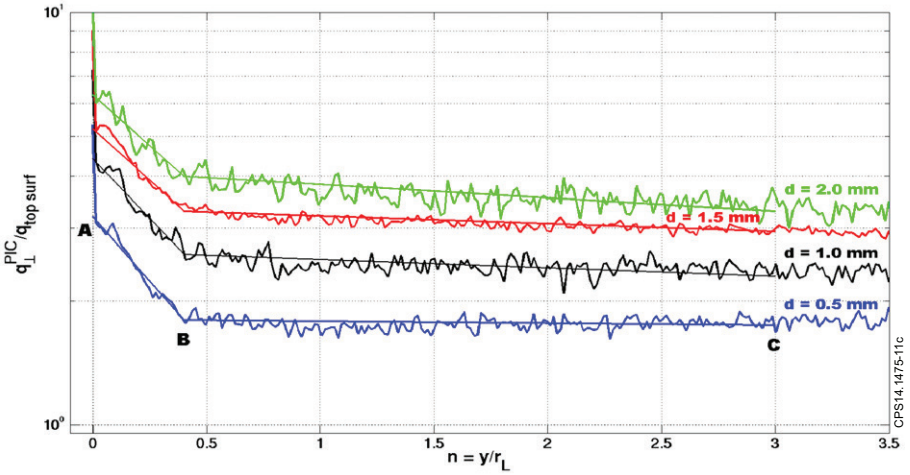

Figure 11: Scaling law for the peak value of the deposited power flux normalized to q_{top_surf} as a function of the misalignment normalized to r_L on the top surface of the lamella for the 3 ELM cases

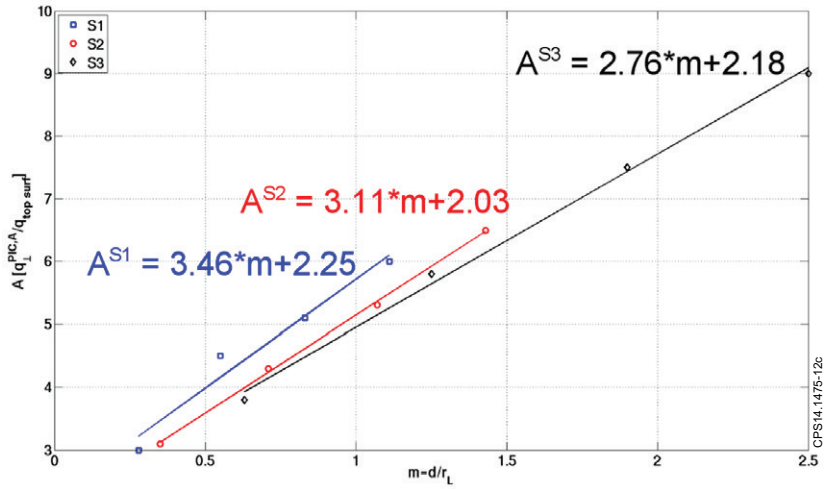

Figure 12: The grid geometry used in the model. Left panel: Volume of the tile. Right panel: Surface condition using constant flux. Blue squares denote the tile volume, red the plasma.

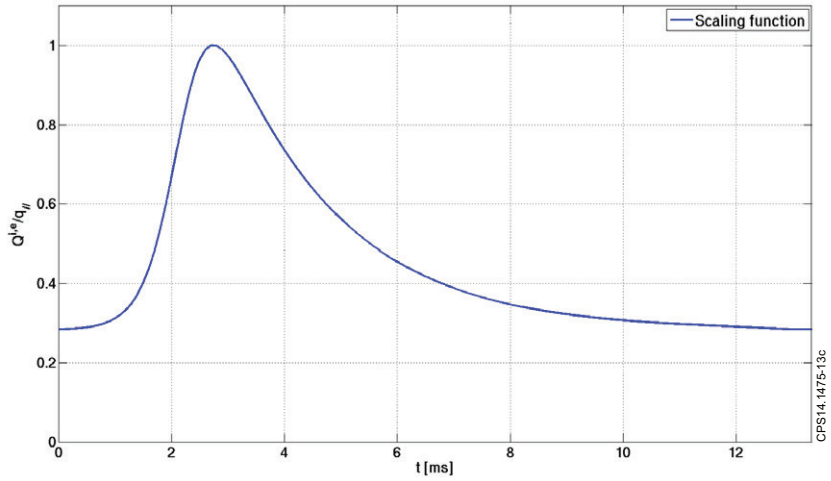

Figure 13: Temporal evolution of the normalized power flux for 1 ELM in JET

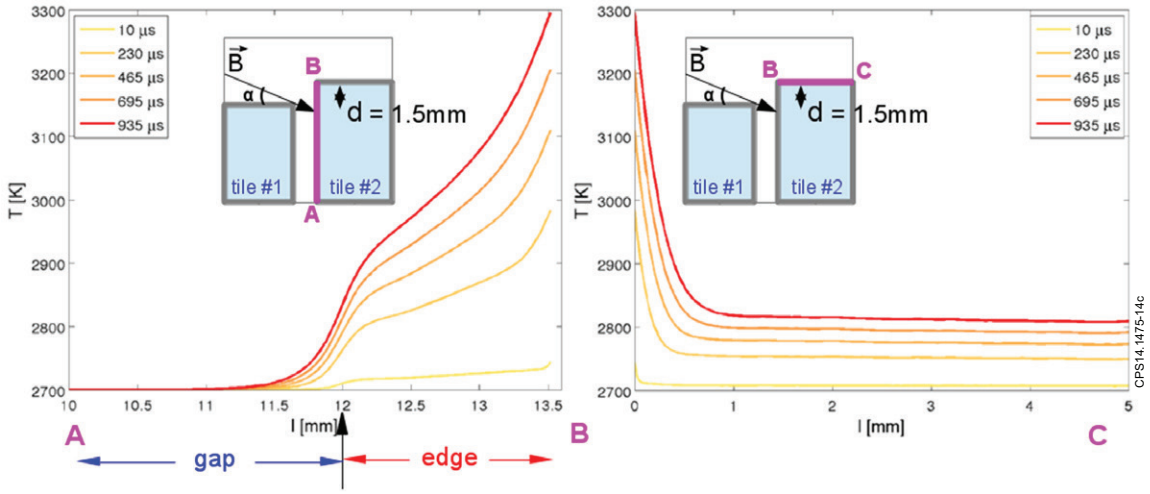

Figure 14: Spatial profiles of the surface temperature on the side (left) and top (right) of the lamella for at different times and for a misalignment of d = 1.5mm for ELM plasma parameters corresponding to Scenario S2

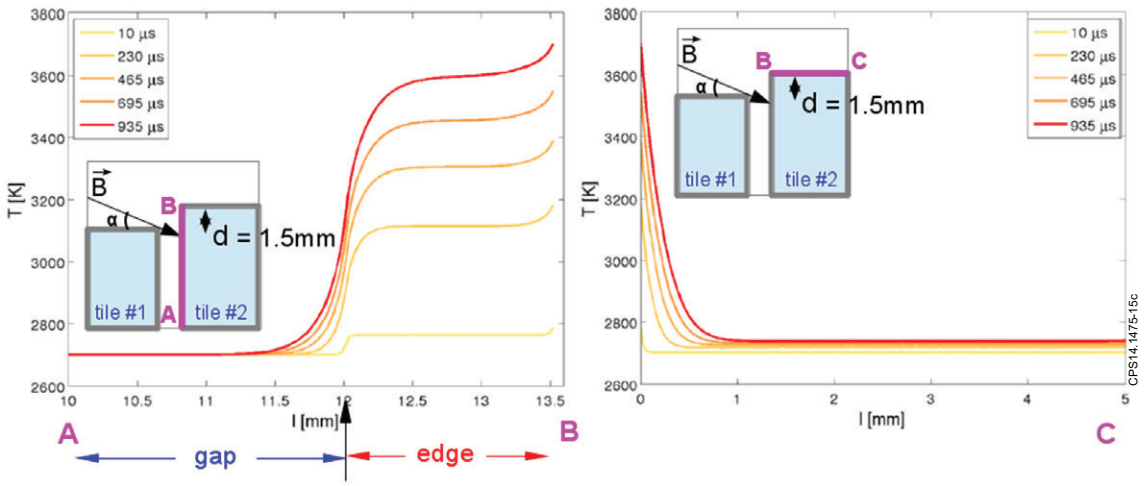

Figure 15: Spatial profiles of the surface temperature on the side (left) and top (right) of the lamella for at different times and for a misalignment of d = 1.5mm for ELM plasma parameters corresponding to Scenario S2

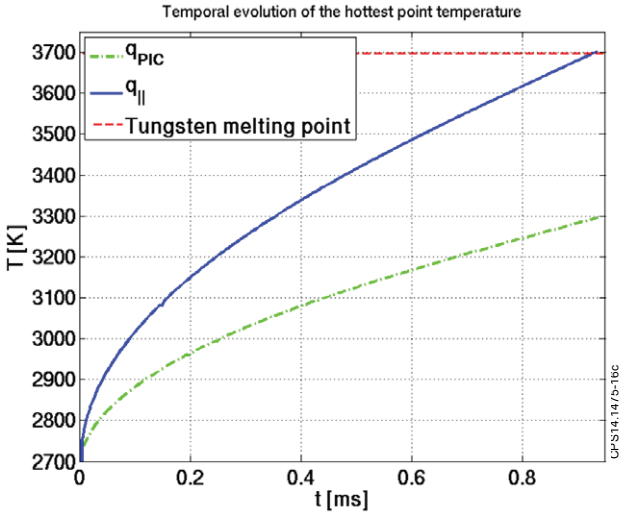

Figure 16: Temporal evolution of T^{surf} of the hottest point for center-guide/ballistic (green) and PIC (blue) power fluxes for the scenario S2 and d = 1.5mm

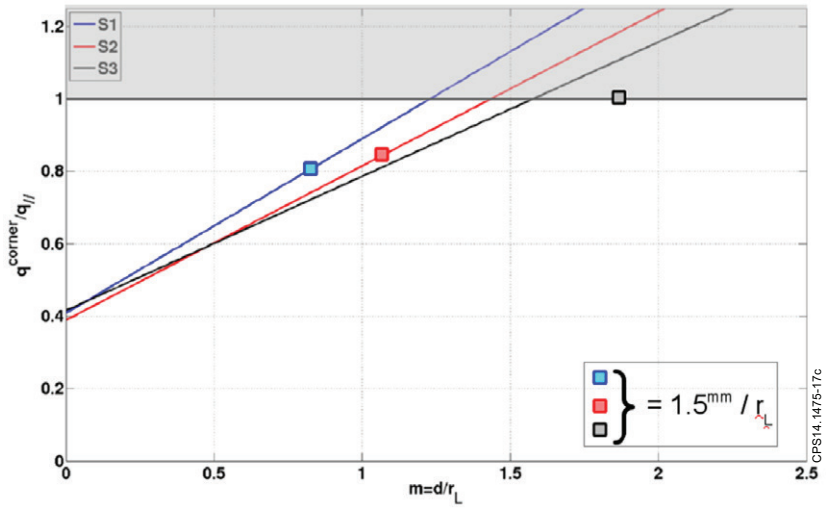

Figure 17: Scaling law for the power flux normalized to $q_{//}$ falling on the corner of the lamella for different ELM scenarios as a function of the misalignment normalized to r_L.